Investigating the source characteristics of long-period (LP) seismic events recorded on Piton de la Fournaise volcano, La Réunion.

Megan Zecevic[a], Louis De Barros[a1], Christopher J. Bean[a], Gareth S. O'Brien[a2], and Florent Brenguier[b]

[a]School of Geological Sciences, University College Dublin, Belfield, Dublin 4, Ireland. E-mail: chris.bean@ucd.ie; megan.zecevic@ucd.ie

[b]Observatoire Volcanologique du Piton de la Fournaise Volcano Observatory, IPGP, 14 RN3-Km27, 97418, La Plaine des Cafres, La Réunion, France. E-mail: florent.brenguier@ujf-grenoble.fr

[1]Present Address: Géoazur, Bât 4, 250 rue Albert Einstein, Les Lucioles 1, Sophia-Antipolis, 06560 Valbonne, France. E-mail: debarros@geoazur.unice.fr

[2]Present Address: Tullow Oil Ltd, Dublin, Ireland. E-mail: Gareth.OBrien@tullowoil.com

_____

Corresponding Author:

Megan Zecevic

School of Geological Sciences, University College Dublin, Belfield, Dublin 4, Ireland (megan.zecevic@ucd.ie). Tel: +353 (0) 1 7162079 Fax: +353 (0) 1 2837733

_____

Abstract

Magmatic and hydrothermal processes play a significant role in generating seismicity at active volcanoes. These signals can be recorded at the surface and can be used to obtain an insight into the volcano's internal dynamics. Long Period (LP) events are of particular interest as they often accompany or precede volcanic eruptions, but they are still not well understood. Piton de la Fournaise volcano, La Réunion Island, is one of the most active volcanoes in the world however LP events are rarely recorded there. A seismic network of 20 broadband seismometers has been operational on Piton de la Fournaise volcano since November 2009. Between November 2009 and January 2011 the volcano erupted five times, but only 15 LP events were recorded. Three of these eruptions were preceded by LP events, and several LP events were recorded during an intrusive phase. A family of three repeating LP events exists within the dataset. In order to characterize these events we locate and perform moment tensor inversion on the LP family. The LP events are located within the summit crater at shallow depths (< 200 m below the surface). Inversions show that the source mechanism is best represented by a tensile crack with horizontal crack geometry. We also investigate the relationship between LP occurrence and eruptive characteristics (size of the eruption, deformation of the edifice, etc.), and we find that the events exist only during flank eruptions and can be generated by the activity of the hydrothermal system and/or by the deformation inside the crater. **Keywords**

Long-period events; Piton de la Fournaise volcano; moment tensor inversion; volcano seismology; seismology

1. Introduction

Long-Period (LP) seismic events, with typical frequencies between 0.5 and 5 Hz, can be seen at many active volcanoes around the world (Chouet, 1996). LP events can be distinguished from other volcano-seismic events by their emergent onset, signal duration, and narrow, peaked spectra (Chouet, 2003). These events are of particular interest as they tend to accompany volcanic eruptions, and are often considered precursors to eruptions, yet they are poorly understood (Chouet, 1996; McNutt, 2005). Due to their association with eruptions it is thought that LP events are associated with fluids moving within the volcano. The most common theory is that they are produced by resonance of a fluid-filled cavity (Chouet, 2003), however the mechanism of excitation of the cavity is unknown and is the subject of various models. For example, Neuberg et al. (2006) suggest that resonance could be triggered in andesitic volcanoes by brittle failure of high viscosity magma with the conduit walls, and Julian (1994) suggests that pressure transients produced by a change in fluid flow or local earthquakes could also potentially trigger resonance. By learning more about the source processes of LP events we can develop a better understanding of the dynamic processes in volcanic systems which could potentially aid in forecasting volcanic eruptions. In order to characterize the LP events, the first step is to locate the events. By locating the events we can gain a better understanding of the geological setting in which they occur. Many location studies (De Barros et al., 2009; Kumagai et al., 2005; Saccorotti et al., 2001; Saccorotti et al., 2007) have found that LP events are typically located at shallow depths (less than 800 m) within the edifice.

Another important character of LP events is their source mechanism. Various studies have related LP events to tensile crack mechanisms, with geometries varying from horizontal to sub-vertical (e.g. Kumagai et al. (2005); De Barros et al. (2011)). Moment tensor inversion

(MTI) has been a useful tool in the last ten years in studying source mechanisms. Moment tensors describe a system of forces that represent the actual physical processes that occur at the source (Aki and Richards, 2002); single forces are also often considered to play a role in the mechanisms of sources within volcanic systems, and have been attributed to mass transfer of material (Takei and Kumazawa, 1995) or drag forces (Ohminato et al., 1998) within the volcano. Complexities in the volcanic environment, such as strong topography and structural heterogeneities, make it difficult to obtain a stable source mechanism (Bean et al., 2008) but inversions have been successfully performed by several authors (Davi et al., 2012; De Barros et al., 2011; Kumagai et al., 2002; Lokmer et al., 2007; Ohminato et al., 1998). Bean et al. (2008) and De Barros et al. (2011) found that for a volcanic environment it is important to use data from dense seismic networks that have been deployed as close as possible to the summit of the volcano in order to obtain good results when performing source inversions for LP events.

Piton de la Fournaise volcano is a basaltic, shield volcano located in the south-east of La Réunion Island in the Indian Ocean, approximately 800 km east of Madagascar (Figure 1 inset). It is associated with the activity of the Réunion hotspot. The summit of Piton de la Fournaise volcano is 2630 m above sea level (a.s.l.), and is characterized by two craters, Bory and Dolomieu. Bory crater is inactive and the smallest of the two craters, whereas Dolomieu is the active crater and was also the site of a large caldera collapse in 2007 (Michon et al., 2007; Staudacher et al., 2009). Piton de la Fournaise volcano is one of the most active volcanoes in the world (Bachelery et al., 1982), with an average of two eruptions per year since 1998 (Peltier et al., 2009); its eruptive activity is comparable to Hawaiian volcanoes with regular emissions of lava and less frequent explosive eruptions. Eruptions on Piton de la Fournaise volcano are

always preceded by intense swarms of volcano-tectonic (VT) events (also referred to as a seismic crisis), which tends to have a duration of a few hours (Aki and Ferrazzini, 2000; Battaglia and Aki, 2003; Battaglia et al., 2005; Nercessian et al., 1996) and indicate magma migrating through the volcano to the surface (Battaglia et al., 2005). LP events have also been recorded during these seismic crises however they are rare in occurrence. For example from 1981 to 1992 Piton de la Fournaise erupted 28 times, however Aki and Ferrazzini (2000) identified only 800 LP events in this period, and in one year, in which there were 5 eruptions, we found only 15 LP events. As Piton de la Fournaise is such an active volcano the number of recorded LP events is surprisingly low in comparison to other active volcanoes. For example during the 2008 Mount Etna eruption more than 500 LP events were recorded in a four day period (De Barros et al., 2009), and 1129 LP events were recorded on Kilauea Volcano, Hawaii during the first few weeks of February 1997 (Almendros et al., 2001).

The VT events recorded on Piton de la Fournaise volcano have been the subject of many studies (Battaglia et al., 2005; Massin et al., 2011; Nercessian et al., 1996), yet very few studies have been carried out on LP events recorded on Piton de la Fournaise volcano. Aki and Ferrazzini (2000) found that LP events were absent in seismic crises that preceded summit eruptions, but were present in all crises that precede flank eruptions. Battaglia and Aki (2003) located the “LP-component” of a hybrid earthquake by inverting the spatial distribution of its seismic amplitude using amplitude decay method. The hybrid earthquake was found to be located around 0.8 km a.s.l, which is approximately 1.8 km below the summit crater.

The aim of this study is therefore to better understand the processes involved in producing these LP events. We also try to determine why so few LP events are recorded on Piton de la Fournaise volcano and whether they are suitable precursors for heralding volcanic eruptions. In this paper we use seismic data recorded from November 2009 to January 2011, from which the LP events are extracted. We will focus on three repeating LP events which we will locate and on which we will perform moment tensor inversion. The results are then compared to geodetic data and put into the context of the eruptive activity.

2. Data

An observatory (Observatoire Volcanologique du Piton de la Fournaise (OVPF)) has been monitoring Piton de la Fournaise volcano since 1980, using permanent seismic and deformation networks (Bachelery et al., 1982). In addition to the permanent seismic network 15 broadband seismic stations were deployed from late October 2009 as part of the Understanding Volcanoes (UnderVolc) project; for instrument specifications see Brenguier et al. (2012). The overall seismic network consisted of 20 seismic stations with three-component broadband sensors, located within the volcano area, with good coverage on the summit (Figure 1); however in this study only 18 seismic stations were used (U02 and HDL were excluded from this study as they malfunctioned during important recording periods).

Five eruptions and an intrusive event were recorded between November 2009 and January 2011, all of which were accompanied by a seismic crisis. Only 15 LP events occurred during this period, and were extracted using an STA/LTA method. All the LP events were

recorded during seismic crises, however not all the eruptions were associated with LP events. Several LP events were recorded during the seismic crisis associated with the intrusive phase on 23rd September 2010 (Figure 2). This phase is called an intrusion as there was no surface eruption but the geodetic and seismic observations reflect those that have been seen in crises that preceded eruptions (Aki and Ferrazzini, 2000).

Before analyzing the data further, we deconvolved the instrument response from the recorded signals and integrate them to obtain accurate values of ground displacement. A high pass filter with a corner frequency of 0.01 Hz was applied to suppress the low frequency noise that was amplified in the deconvolution process. The seismic signals were also corrected for site amplification effects determined by normalizing the RMS amplitude of the coda waves of a teleseismic magnitude 6.3 earthquake (approximately 1100 km away) filtered between 0.5 and 4.0 Hz.

Most of the energy of the 15 LP events is concentrated between 2.0 and 4.0 Hz, and as is typical for LP events the P- and S-phases are difficult to differentiate as they are recorded in the near-field (Figure 3). The LP events also have long waveforms (10-12 s) which suggest that they either have a complex source or that they are strongly affected by path effects (Bean et al., 2008). A family of 3 LP events (LPs 4, 5 and 7) recorded during the September 2010 intrusion was found within the dataset. These events are known as a family because at each single station the recorded events are well correlated (Figure 4), with a minimum correlation coefficient of 0.71 between LPs 4 and 5 at station U04 and correlation coefficients > 0.9 between all three events on

the summit stations, thus it can be assumed that the family of LP events share very similar source locations and mechanisms. A family of 3 events is small in comparison to families that have been observed on other volcanoes such as Soufrière Hills Volcano, Montserrat, where 6 families containing at least 45 events each were recorded in a 48 hour period (Green and Neuberg, 2006). Studying such a small family however could potentially provide new insights as to why LP events on Piton de la Fournaise are so rare.

3. Location

LP events are difficult to locate using conventional earthquake location methods due to their emergent onsets and lack of clearly separated P- and S-waves (Chouet, 2003), however on the La Réunion data first-arrival times can be picked on some stations. An initial location for the family of LP events is found using a classical travel time method with all available stations (Saccorotti et al., 2007), the results of which are shown in Figure 5. The sources of the events are shallow, but more scattered than expected for events with such similar waveforms. Due to the imprecision of picking the onset of an event, especially at the furthest stations, we take advantage of the similarity between waveforms to determine the source location. Preliminary time-picks of P-waves and the differential travel times between similar events, obtained through waveform cross-correlation, can be used together to improve the location of a cluster of earthquakes in a double-difference method (Got et al., 1994; Shearer, 1997; Waldhauser and Ellsworth, 2000).

149 The double-difference method described by Shearer (1997) and Waldhauser and
150 Ellsworth (2000) has been adapted to locate the family of 3 LP events recorded on Piton de la
151 Fournaise volcano, whose individual waveforms differ from station to station but are well
152 correlated at single stations, as illustrated in Figure 4. In our adaptation, rather than adjusting the
153 picked times separately for each station, the differential time between event picks for pairs of
154 stations are adjusted. This method requires the picked first-arrival times and the cross-correlated
155 differential travel times to be compared for all pairs of stations to obtain differential pick times
156 and double-differential cross-correlated travel times (also called differential delay times). The
157 advantages of this method are (1) that knowledge of an absolute location is not required as
158 typical for other double-difference methods (Waldhauser and Ellsworth, 2000), (2) that it allows
159 for errors in first-arrival times, and (3) that a reference origin time for each event is not required
160 as differential times are used.

161

162 For a specific example of 3 clustered events, as seen in this study, recorded on a single
163 pair of stations, A and B, the relationship between the differential (pick and delay) times and the
164 model of adjusted differential pick times can be explicitly written as:

$$\begin{bmatrix} \Delta T_1^{AB} \\ \Delta T_2^{AB} \\ \Delta T_3^{AB} \\ \Delta T_{12}^{A} - \Delta T_{12}^{B} \\ \Delta T_{13}^{A} - \Delta T_{13}^{B} \\ \Delta T_{23}^{A} - \Delta T_{23}^{B} \end{bmatrix} = \begin{bmatrix} 1 & 0 & 0 \\ 0 & 1 & 0 \\ 0 & 0 & 1 \\ 1 & -1 & 0 \\ 1 & 0 & -1 \\ 0 & 1 & -1 \end{bmatrix} \cdot \begin{bmatrix} \Delta t_1^{AB} \\ \Delta t_2^{AB} \\ \Delta t_3^{AB} \end{bmatrix} \quad \textbf{(1)}$$

where ΔT_i^{AB} is the time difference between pick times at station A and B for event i; ΔT_{ij}^{A} is the delay time between events i and j, determined from cross-correlation of part of the waveforms associated with the beginning of the event, recorded at station A; Δt_i^{AB} is the adjusted differential pick time for event i between stations A and B, obtained by solving Equation 1. This is done by using a weighted least-squares solution; the weight vector contains a given value according to the picking quality and correlation coefficient between waveforms.

For the location procedure a homogeneous velocity model of the volcano was used which assumes spherical wavefront propagation due to the short distances between source and receivers. The velocity used was 3500 ms^{-1} as it corresponds to the velocity of the uppermost layer (almost the entire thickness of the volcano above sea level) of an 8 layer velocity model used for routine location of VT events at the OVPF (Battaglia et al., 2005). The model (24.8 km x 17.5 km x 2.6 km) was discretised into a regularly spaced grid with a resolution of 25 m. Theoretical differential travel times were then calculated from each grid point to all pairs of stations. The most probable source location for each event is the grid point which yields the minimum misfit between the theoretical differential travel times and the adjusted differential pick times, Δt_i^{AB}, determined by Equation1 for all pairs of stations.

The locations of the family of LP events calculated with this method can also be seen in Figure 5. Error bars were calculated to show the extent of locations that had a misfit within 5% of the misfit value of the most probable location. Contrary to the locations obtained using first arrival times, the hypocenters of the LP events obtained by the modified double-difference

187 method are found clustered together. Moreover, the uncertainty of the location is greatly reduced,
188 from more than 500 m to less than 100 m, illustrating the imprecision associated with picked first
189 arrival times. The events are located within the Dolomieu crater, at a very shallow depth just 50
190 m below the surface. To determine the stability of the hypocenters, the location process was
191 reiterated for other homogenous velocities between 3000-3500 ms^{-1}. The epicenters of the LP
192 events are well resolved with horizontal variations no greater than 125m, the depth of the sources
193 are more sensitive to the different velocities however they remain shallow and are located no
194 more than 500 m below the crater, but are likely to be less than 200 m deep.

195

4. Moment Tensor Inversion (MTI)

4.1. Method

196 A recorded seismogram contains information about both the source process and the
197 response of the Earth due to the seismic wave propagating from the source to the receiver. This
198 can be estimated using elastic Green's functions, and can be described in the frequency domain
199 as (Aki and Richards, 2002; Ohminato et al., 1998):

$$\mathbf{u}_n(s,f) = \mathbf{M}_{pq}(f).\mathbf{G}_{np,q}(s,f) + \mathbf{F}_p(f).\mathbf{G}_{np}(s,f) \qquad n,p,q = x,y,z \qquad \textbf{(2)}$$

200 where $u_n(s,f)$ is the n^{th} component of the displacement, recorded at position s and frequency f;
201 M_{pq} is the force couple or dipole in the pq direction acting at the source; F_p is the single force
202 acting in the p direction; G_{np} and $G_{np,q}$ represent the n^{th} components of the Green's functions
203 and their derivatives, respectively. Note that x, y, and z refer to the east, north and vertical
204 components, respectively.

Equation 2 shows that the robustness of the inversion result is strongly dependent on the accuracy of the calculated Green's functions (Bean et al., 2008). In this study, the Green's functions are calculated using full-waveform simulations of seismic wave propagation from a point-source to each receiver using an elastic lattice method (O'Brien and Bean, 2004), with a Gaussian pulse as the source-time function. In order to save on computational costs the model in which the simulations run is cropped, thereby removing station U01 (Figure 1) and reducing the number of stations used in the MTI to 17. Many studies jointly invert for both source location and mechanism, however Lokmer et al. (2007) found that in joint-inversion there was a trade-off between location and mechanism when the shallow velocity model is poorly resolved. The locations obtained using the double difference method above for the family of LP events are therefore used. However rather than running Green's functions calculations for three events that are tightly clustered together, only one source location is used, which is determined by averaging the epicenters of the three LP locations shown in Figure 5. As the source depth is poorly constrained, Green's functions are computed for source depths of 50 m, 200 m and 500 m below the surface. The topography of Piton de la Fournaise volcano is also included in the Green's functions computation. A high-resolution velocity model does not currently exist for the shallow part of Piton de la Fournaise volcano, therefore a homogenous velocity model, with P-wave velocity of 3500 ms^{-1} and S-wave velocity of 2000 ms^{-1}, is used for the Green's functions calculation, which is consistent with the velocity model used in the location method above.

The moment tensor is assumed to be symmetrical, with $M_{pq}(f) \equiv M_{qp}(f)$, therefore only six moment tensor components need to be determined. De Barros et al. (2011) found that a more stable moment tensor solution is found when single forces are included in the inversion process than when inverting without single forces, as some of the errors resulting from mislocation of the source and/or from an incorrect velocity model are accommodated within the single forces solution. It is therefore not obvious whether any recovered single forces are real or an artifact of the Green's functions calculation or source location. Hence, in order to obtain a stable moment tensor solution, single forces were included in the inversion process when inverting each of the LP events but only the moment tensor solution is analyzed.

Equation 2 shows that retrieving the source function is a linear inverse problem in the frequency domain, and can be written simply in matrix form as:

$$\boldsymbol{d} = \boldsymbol{G}\boldsymbol{m} \qquad \textbf{(3)}$$

where d is the displacement seismograms recorded at each station, merged into a column vector; G is a matrix containing the Green's functions and their derivatives; and m is a column vector containing the unknowns, i.e. the moment tensor components and single forces.

Although the dominant frequency of the events is between 2 and 4 Hz, we focus on a lower frequency part of the data with significant energy (0.7 - 1.8 Hz) as lower frequencies are less sensitive to error in the velocity model (Kumagai et al., 2011). Equation 3 can then be solved for each frequency using a least squares approach. The waveform misfit function is defined by:

$$Misfit = \frac{(\boldsymbol{d}-\boldsymbol{Gm})^{\boldsymbol{T}}(\boldsymbol{d}-\boldsymbol{Gm})}{\boldsymbol{d}^{\boldsymbol{T}}\boldsymbol{d}} \quad \textbf{(4)}$$

The inversion results in six frequency functions (nine if single forces are included in the MTI) which best fit the data, which are converted into six/nine independent source-time functions by applying an inverse Fourier transform. These source-time functions can then be decomposed into their eigenvalues and eigenvectors by performing principle component analysis to determine the source mechanism and orientation, respectively (Vasco, 1989).

4.2. Results of the MTI

MTI including single forces for the three relocated LP events is carried out assuming a source depth of 50 m. Results for LP 5 can be seen in Figure 6. The LP event source can be described by a moment tensor approximated by $[M_{xx} = 1; M_{yy} = 1; M_{zz} = 3;\ M_{xy} = M_{xz} = M_{yz} = 0]$, with strong isotropic and compensated linear vector dipole (CLVD) components (Table 1) (Vavrycuk, 2001). Hence the source mechanism can best be described as a sub-horizontal tensile crack assuming that the two Lamé parameters are equal (i.e. $\lambda \equiv \mu$) (Bean et al., 2008). As expected for events with similar waveforms the mechanisms are negligibly different for all three events. The waveform misfit value is 0.63 (Table 1); the waveforms recorded on the three summit stations, U05, U11 and SNE, are very well reconstructed as demonstrated in Figure 6b, which is important as they have the largest amplitudes and are thus most likely to influence the results of the MTI. In order to determine the robustness of the source orientation, eigenvectors are calculated for each data point on the source-time functions with amplitude greater than 80% of the maximum amplitude; Figure 6c shows that the orientation of

266 the crack for all the LP events is well defined, with the principle axis tilted at an average angle of
267 3-5° from vertical.

268

269 The maximum amplitude of the moment tensor components is of the order 10^{11} Nm,
270 while the single forces have maximum amplitude of the order 10^{7} N (Figure 6a); the latter are
271 therefore only responsible for a small amount of the seismic waveforms. To check the stability of
272 the solution, we also perform MTI without single forces. The results are given in Table 1, and
273 show the same mechanism as the inversion including single forces; this is a confirmation of the
274 stability of the moment tensor solution (De Barros et al., 2011).

275

276 As the moment tensor solution suggests a crack mechanism, the data is inverted for a
277 constrained crack mechanism to determine the azimuth angle, φ, and dip angle, θ, of the axis of
278 symmetry for each of the Cartesian components of the moment tensor (Lokmer et al., 2007;
279 Nakano and Kumagai, 2005). We use the expression of M_{pq} derived by De Barros et al. (2011)
280 and Nakano and Kumagai (2005) to constrain the inversion for a crack. M_{pq} are dependent on
281 the seismic moment M_0, Lamé parameters λ and μ, dip angle θ, measured from 0° to 90° from
282 the upward vertical direction, and the azimuth angle, φ, measured between 0° and 360°
283 anticlockwise from east.

284

285 For each frequency a grid search is performed for the most probable solution in the θ- φ
286 domain. The constrained inversion has thus only one free unknown, M_0. The results of the

287 constrained inversion show that the crack orientation that best fits the data is also a sub-
288 horizontal crack (Table 1), which confirms the results of the unconstrained moment tensor
289 inversion solutions.
290
291 As mentioned previously, the amplitude of the LP waveforms recorded on the three
292 summit stations is much greater than those recorded on the other stations, and can therefore
293 strongly influence the MTI. In order to test the sensitivity of the crack solution to these summit
294 stations we perform a jackknife test by removing one or more of these stations and perform the
295 inversion again. The solution is found to be stable giving us confidence in the reconstructed
296 source mechanism.
297
298 **4.4. Sensitivity to source depth and velocity model**
299 As shown in the location section, the horizontal location is very well constrained, while
300 the depth of the source is less well resolved. Joint inversion for the mechanism and the location
301 through a grid search could have been performed, however a trade-off might exist between both
302 unknowns, leading to spurious solutions at the wrong location (Lokmer et al., 2007). This is
303 particularly true when the near-surface velocity model is not known (Bean et al., 2008) and for
304 high frequencies (Kumagai et al., 2011). We therefore took advantage of the well constrained
305 source location, and just need to check how sensitive the solution is to an error in depth. We
306 therefore calculate Green's functions for source depths of 200 m and 500 m and compare them
307 with the solutions obtained above for 50 m depth. Moment tensor inversions including single
308 forces are performed for each LP event and analyzed the same as above. For a source depth of
309 200 m, the LP events produce a moment tensor solution approximated by $[M_{xx} = 1; M_{yy} =$

310 $1; M_{zz} = 5;\ M_{xy} = M_{xz} = M_{yz} = 0]$ (Table 1) which cannot be clearly interpreted as a simple
311 source mechanism. However, when one or more of the summit stations were removed from the
312 inversion process the solution became a $[M_{xx} = 1; M_{yy} = 1; M_{zz} = 3]$ solution (Table 1). A
313 crack constrained inversion leads to a solution similar to the one found at 50 m depth. The
314 misfits are similar for an unconstrained and crack constrained inversion at 50 and 200 m depth,
315 however the 200 m deep solution suffer from 1) an increase in the single forces and 2) moment
316 tensor components which are out-of-phase. These two points reveal a source mislocation or an
317 error in the velocity model.
318
319 The MTI results for a source depth of 500 m are even more unstable, with very high
320 single forces and out-of-phase components. The misfit is higher than at 50 m and 200 m, which
321 discards this depth as a possible solution.
322 As mentioned previously if an incorrect velocity model is used during MTI, errors can
323 leak into the moment tensor solution. Using a homogenous velocity model is not ideal as
324 volcanoes often have a shallow, low velocity layer which can significantly alter the Green's
325 functions (Bean et al., 2008). In order to test the sensitivity of the moment tensor solution to
326 variations in the velocity model a more complex velocity model is required. As a detailed
327 velocity model does not exist for the shallow part of Piton de la Fournaise, a layered velocity
328 model, constrained by the shallow velocity of Kilauea volcano, Hawaii (Saccorotti et al., 2003)
329 (which is a similar volcano to Piton de la Fournaise in terms of behavior and magma chemistry),
330 is used. Saccorotti et al. (2003) suggest a shear wave velocity for Kilauea volcano of
331 approximately 1200 ms^{-1} in the top 100-200 m which increases to approximately 2000 ms^{-1} at
332 400 m depth. Hence the corresponding velocity model used here consists of a shallow layer 400

m thick with a constant velocity gradient: the P-wave velocity at the surface is 2000 ms^{-1} and increases steadily to 3500 ms^{-1} at the bottom of the layer. Beneath the layer the velocity remained homogenous at 3500 ms^{-1}.

The results from the MTI using this layered velocity model are out of phase for the 50 m source depth, but the results for the 200 m source depth gives the same mechanism as the results for the homogenous model and is depicted by a horizontal crack. The amplitude ratio between the single forces and the moment tensor is much larger for the solutions with the layered velocity model compared to the homogeneous velocity model, which suggests that the homogeneous model is more suitable to perform MTI on Piton de la Fournaise. Hence the results using the homogeneous model are taken as the most reliable until better constraints are available for the near-surface velocity of Piton de la Fournaise.

The various tests show that the results of the moment tensor inversions are much more stable for shallow source depths of 50 m and 200 m, and although it is not possible to give a highly constrained source depth due to a poor velocity model, the MTI results imply that the source depth is very shallow beneath the summit crater. This result is consistent with the locations determined using the modified double-difference method described above. In conclusion, the source mechanism of the LP events can be depicted by a shallow horizontal tensile crack. The magnitude of the seismic moment of the family of LP events at 50m depth varies from $3 \cdot 10^{11}$ Nm to $7 \cdot 10^{11}$ Nm, therefore the volumetric change, ΔV, of the crack to produce the family of LP events is estimated, using $M_0 = \mu \Delta V$, to be within the range of 30-70

355 m^3. This crude approximation assumes that the rigidity of the medium, μ, used in the Green's
356 functions calculations is equivalent to the rigidity of the source region.

5. Discussion

357 Piton de la Fournaise is one of the most active volcanoes in the world, yet LP events are
358 seldom recorded here. A family of 3 LP events was found to be located within the top 200 m of
359 the volcano with a source mechanism best described as a horizontal crack. In order to understand
360 the role of LP events during eruptions we look at factors such as the generation of LPs in time
361 and space and their relationship with other volcano-seismic events during eruptions on Piton de
362 la Fournaise volcano. We also compare characteristics of Piton de la Fournaise with other
363 volcanoes to further understand why LP events rarely occur here.

364

5.1 Eruptions with and without LP events

365 LP events were only recorded during three of the six seismic crises analysed, two of
366 which preceded eruptions in November 2009 and October 2011, and one which occurred during
367 the intrusive phase in September 2010 (Figure 2); hence LP events cannot be used to
368 differentiate between intrusive and eruptive phases on Piton de la Fournaise volcano. All the
369 eruptions and intrusions are associated with significant deformation of the volcano's edifice
370 before and during eruptions (Peltier et al., 2007), therefore there does not appear to be a distinct
371 correlation between deformation and the occurrence of LP events. For each of the eruptions the
372 lavas are similar with typical pahoehoe and aa type flows, however the volume of erupted lava
373 can vary between eruptions by an order of magnitude. There also does not appear to be a
374 correlation between the volume of extruded material and LP occurrence; for example the total

volume of lava emitted during the November and December 2009 eruptions was approximately $1.4 . 10^5$ m^3 and $1.6 . 10^5$ m^3, respectively, and the total amount of lava extruded in January 2010 was approximately $1.4 . 10^6$ m^3 (OVPF report, 2010), yet LP events were not recorded during either the December or January eruptions.

The most obvious relationships between LP occurrence and eruptions are (1) where the eruption occurs on the volcano; and (2) the length of time between consecutive eruptions. First, three types of eruptions have been distinguished on Piton de la Fournaise volcano: summit eruptions that occur within Dolomieu crater, proximal eruptions that begin close to the summit but migrate down slope onto the flanks of the central cone, and distal eruptions which occur at distances greater than 4km from the summit cone (Peltier et al., 2009). November 2009, October 2010 and December 2010 were proximal eruptions whereas December 2009 and January 2010 were summit eruptions; hence our findings concur with those of Aki and Ferrazzini (2000) that LP events are only associated with proximal eruptions rather than summit eruptions. This observation is important when monitoring the volcano, as the occurrence of LP events during a seismic crisis could indicate that the eruption will occur on the flanks of Piton de la Fournaise volcano.

Second, LP events are recorded at the beginning of a new series of eruptions, after a lull of several months in eruptive activity. For example the eruption prior to the November 2009 eruption occurred over a year before in September 2008 (Staudacher, 2010), and the October 2010 eruption occurred 9 months after the January 2010 (Figure 2). This suggests that the state

of the volcano is different at the beginning of an eruptive series (e.g. November 2009) than during (e.g. December 2009) or towards the end of the series (e.g. January 2010). This could be indicative of a change in the property of volcanic fluids or in the stress field on the volcano. As the data only spans two eruptive series we are unable to fully determine if there is a temporal trend between LP activity and all eruptive series.

5.2 Volcano-Tectonic (VT) versus Long Period (LP) Events

Pre-eruptive activity on Piton de la Fournaise volcano generally follows the Generic Volcanic Earthquake Swarm Model described by McNutt (2000). A typical seismic crisis on Piton de la Fournaise volcano consists of a dense swarm of VT events with a duration of several hours followed by a short period of relative seismic quiescence, which can then lead to either volcanic tremor originating from the eruption site or normal background seismicity indicating the crisis was the result of an intrusion. LP events are usually recorded towards the end of the seismic crises, after the seismicity rate peaks and just before the quiescent phase (Aki and Ferrazzini, 2000) (Figure 7).

The hypocenters of LP events are much shallower than VT events recorded during the seismic crises on Piton de la Fournaise volcano. As mentioned previously, the LP events are located at shallow depths within the Dolomieu crater, which was reformed in 2007 due to a caldera collapse. However during an eruption in 2008, pahoehoe and aa-type lava flowed into the crater raising the crater floor by up to 50 m (Staudacher, 2010). Several eruptions, ash plumes and minor debris flows have also occurred since then (Venzke et al., 2010); therefore it is possible

418 that the LP events recorded are located within this unconsolidated material or at the interface
419 between this material and the stiff basalt, which forms the volcanic edifice. The VT events are
420 located in clusters beneath the central cone at depths below 0.8 km a.s.l. (Aki and Ferrazzini,
421 2000; Massin et al., 2011). A semi-aseismic zone appears to exist between 0.8 km a.s.l. and 2 km
422 a.s.l., above which the LP events are located. This zone is not completely devoid of seismicity as
423 several VT events (Massin et al., 2011) and a hybrid event (Battaglia and Aki, 2003) were
424 located within this zone however they do not occur in large numbers.

425

5.3 How does Piton de la Fournaise volcano vary to other volcanoes?

426 LP seismicity is very sparse on Piton de la Fournaise volcano compared to other
427 volcanoes, e.g. Kilauea volcano (Almendros et al., 2001) and Mount Etna (Lokmer et al., 2007).
428 Two main differences can be identified between Piton de la Fournaise volcano and other
429 volcanoes. First, as LP events are often associated with fluids within the volcano (Chouet, 2003)
430 a possible explanation for the lack of LP events on Piton de la Fournaise volcano could be
431 associated with the fluid properties and their systems. The volume of volcanic gas emitted during
432 eruptions on Piton de la Fournaise volcano is quite low, and little to no gas is emitted during
433 times of quiescence. As typical for mafic lava the viscosity of lava on Piton de la Fournaise is
434 low which is evident in the Pahoehoe-type lava flows. Kilauea volcano also shows Hawaiian-
435 type eruptive activity with Pahoehoe and aa lava flows similar to those observed at Piton de la
436 Fournaise, yet numerous LP events are recorded there (note that this is a qualitative description
437 and provides no constraint on either composition or viscosity of the lava flows). A mature
438 hydrothermal system exists in Kilauea volcano, and many studies suggest that LP activity on

Kilauea has a hydrothermal origin (Almendros et al., 2001; Kumagai et al., 2005; Saccorotti et al., 2001). Various studies suggest that a hydrothermal system may exist within Piton de la Fournaise (Gouhier and Coppola, 2011; Lénat et al., 2000; Peltier et al., 2012) however there is no clear evidence to confirm this. The lack of evidence for a hydrothermal system could suggest that the hydrothermal system at Piton de la Fournaise, if it exists, is not as well-developed as that on Kilauea; therefore there will be less interaction between the hydrothermal and magmatic systems, which could potentially explain the lack of LP event generation.

The second difference is linked to the mechanical properties of the volcano's edifice. Volcanoes such as Etna are typically built with poorly consolidated material, consisting of alternating layers of lava, ash and pyroclastic deposits. The velocity in the shallow medium is therefore very slow, with P-wave velocity no more than 1800 ms^{-1} in the top 400 m (Saccorotti et al., 2004) where LP events are generated (De Barros et al., 2009). In contrast, Kilauea volcano is built of basalt but a shallow low velocity layer, which is slightly higher in velocity than Etna, does exist (Saccorotti et al., 2003). Similarly to Kilauea, the cone of Piton de la Fournaise volcano is composed of layers of stiff basalt (Peltier et al., 2009) (with an average P-wave velocity greater than 3000 ms^{-1} (Battaglia et al., 2005; Nercessian et al., 1996)), but it is unknown if a shallow, low velocity layer exists on this volcano. The strength of the material reflects how easy it is for a crack to open/close; therefore the lack of a low velocity layer could potentially explain why less LP events are recorded on Piton de la Fournaise, as horizontal cracks required for LP event generation may not be able to open/close on Piton de la Fournaise as readily as other volcanoes. The length of the LP signals (10-12 seconds) on Piton de la Fournaise suggests that a strong impedance contrast exists between the fluid inside the crack and

462 the surrounding solid. A high impedance contrast can be explained by the presence of a low-
463 velocity fluid surrounded by a high velocity medium, however there are too many unknown
464 parameter to constrain the type of fluid within the crack. Hence a detailed near-surface velocity
465 model of Piton de la Fournaise could be beneficial in comparing Piton de la Fournaise with other
466 volcanoes.

5.4 Potential Models

467 As the seismic crises recorded on Piton de la Fournaise volcano are associated with
468 magma upwelling through the volcano (Aki and Ferrazzini, 2000), the type of seismicity
469 recorded during the seismic crises could be associated with the magma front. Taisne et al. (2011)
470 imaged magma migration before an eruption by locating the radiated seismic energy of a seismic
471 crisis. During flank eruptions, two phases of magma migration were distinguished by Peltier et
472 al. (2005) using tiltmeter measurements. The first phase relates to the inflation of the summit
473 within the first few minutes of a seismic crisis describing the vertical injection of magma.
474 Therefore it is possible that as magma propagates vertically from sea level to 0.8 km a.s.l., where
475 the material is compact and highly pressurized, the stress perturbations produce a series of VT
476 events that occur in quick succession. Then as the magma passes into the semi-aseismic zone the
477 rate of recorded seismicity decreases. The second phase of magma migration relates to lateral
478 inflation of the flank and summit deflation as the magma propagates laterally to the eruption site
479 (Peltier et al., 2005).

480

481 On Kilauea, Almendros et al. (2001) and Kumagai et al. (2005) proposed that rising
482 magma reactivates the shallow hydrothermal system, thus increasing the pressure within the
483 hydrothermal system. When the pressure reaches a critical limit, fluid is rapidly discharged from
484 the hydrothermal crack thereby triggering resonance and hence producing LP events. Magmatic-
485 hydrothermal interactions have also been suggested as LP source machanisms on other volcanoes
486 (e.g. Arciniega-Ceballos et al. (2012) on Popocatepetl; Matoza and Chouet (2010) on Mt St
487 Helens). A similar hypothesis can be considered here: the upwelling magma could regenerate the
488 shallow hydrothermal system, and pressure will begin to build up in the system. The scarcity of
489 LP events on Piton de la Fournaise compared to Kilauea could be explained by the differences in
490 maturity and the extent of the hydrothermal systems. Moreover, during an eruptive series a small
491 hydrothermal system may not replenish fully due to high evaporation rates, however the lull
492 between separate eruptive series would allow the hydrothermal system to refill. This could
493 potentially explain why LP events were only recorded at the beginning of an eruptive series.
494 Unfortunately heating of the hydrothermal system does not fully explain the generation of LP
495 events on Piton de la Fournaise however, as it does not account for why LP events are not
496 generated during summit eruptions.

497

498 Another hypothesis to explain the LP generation is linked to the deformation cycles
499 associated with the lateral propagation of the magma (Peltier et al., 2005). Summit deflation, due
500 to a release of pressure under the summit as the dyke propagates to the flank, may potentially
501 result in the closing of a horizontal crack which could eject hydrothermal fluid and hence
502 theoretically produce LP events. This follows on from observations by Chouet (1996) and *De*
503 *Barros et al.* [2011] that LP events are often recorded during deflation episodes of the summit at

Kilauea and Mount Etna, respectively. The unconsolidated material near the summit of a volcano, where the LP events are located, would have a lower confining pressure than compacted material deep within the volcano, where the VT events are located, and therefore would allow mode I fractures to occur more readily (Fischer and Guest, 2011).

While opening/closing of cracks are possible within compliant materials, it is more difficult when the medium is made of stiff rock. This potentially could justify why LP events only transpire within the summit crater of Piton de la Fournaise volcano, where the material is compliant and the confining pressure is low. Hence, the mechanical properties of the edifice combined with an under-developed hydrothermal system could explain why so few LP events are recorded on Piton de la Fournaise compared to other volcanoes. However, because of the small number of events generated on this volcano, the interpretation of the processes which generate them is delicate. Additional data are therefore needed to improve the understanding of their sources.

6. Conclusion

LP events are rare on Piton de la Fournaise volcano; 5 eruptions and an intrusion occurred between November 2009 and January 2011, yet only 15 LP events were recorded. A family of LP events accompanying the intrusion was identified and located, using a modified double-difference method, at a shallow depth (< 200 m) beneath the Dolomieu crater. Moment tensor inversions attributed the source mechanisms of the family of LP events to the opening/closing of a horizontal tensile crack and further agree with a shallow source location. LP

525 events are typically recorded towards the end of a seismic crisis, after a series of VT events,
526 however the source of LP events differ in location to VT events.

527

528 LP events cannot be used to differentiate between intrusions and eruptions on Piton de la
529 Fournaise volcano, but appear to only accompany proximal eruptions that occur on the flank of
530 the summit cone. This observation could potentially be used for forecasting the location of the
531 eruption. The association of LP events with flank eruptions could be related to reactivation of a
532 hydrothermal system and/or changes in the stress field on the volcano during flank eruptions.
533 During proximal eruptions magma propagates vertically upwards where it could reheat the
534 shallow hydrothermal system before migrating laterally to the flanks (Peltier et al., 2005). The
535 migration laterally is accompanied by a short, rapid deflation of the summit which could explain
536 the horizontal crack mechanism that produces LP events. We hypothesize that the LP events are
537 generated in the crater material as a response to the summit deflation preceding lateral eruptions,
538 which can cause a hydrothermal crack to discharge fluid and close, leading to impulsive
539 excitation and resonance. Except inside the crater, the edifice of Piton de la Fournaise volcano is
540 made of stiff basalt, where tensile crack mechanisms are less likely to occur. We suggest that
541 this, combined with an under-developed hydrothermal system, are the main reasons why so few
542 LP events occur on Piton de la Fournaise volcano.

543

Acknowledgements

544 We gratefully acknowledge support from the European Commission (Marie Curie Actions, ITN
545 QUEST, www.quest-itn.org). The data used for the analysis were collected by the Institut de

Physique du Globe de Paris, Observatoire Volcanologique du Piton de la Fournaise (IPGP/OVPF), and the Institut des Sciences de la Terre (ISTerre) within the framework of ANR_08_RISK_011/UnderVolc project. The sensors are property of the French transportable seismic network, Sismob (INSU-CNRS). We also wish to acknowledge the SFI/HEA Irish Centre for High-End Computing (ICHEC) for the provision of computational facilities and support.

References

Aki, K. and Ferrazzini, V., 2000. Seismic monitoring and modeling of an active volcano for prediction. J. Geophys. Res., 105(B7): 16617-16640.

Aki, K. and Richards, P.G., 2002. Quantitative seismology. University Science Books, Sausalito, California.

Almendros, J., Chouet, B. and Dawson, P., 2001. Spatial extent of a hydrothermal system at Kilauea Volcano, Hawaii, determined from array analyses of shallow long-period seismicity 2. Results. J. Geophys. Res., 106(B7): 13581-13597.

Arciniega-Ceballos, A., Dawson, P. and Chouet, B.A., 2012. Long period seismic source characterization at Popocatépetl volcano, Mexico. Geophysical Research Letters, 39(20): L20307.

Bachelery, P., Blum, P.A., Cheminee, J.L., Chevallier, L., Gaulon, R., Girardin, N., Jaupart, C., Lalanne, F., Le Mouel, J.L., Ruegg, J.C. and Vincent, P., 1982. Eruption at Le Piton de la Fournaise volcano on 3 February 1981. Nature, 297(5865): 395-397.

566 Battaglia, J. and Aki, K., 2003. Location of seismic events and eruptive fissures on the Piton de
567 la Fournaise volcano using seismic amplitudes. J. Geophys. Res., 108(B8): 2364.

568 Battaglia, J., Ferrazzini, V., Staudacher, T., Aki, K. and Cheminée, J.-L., 2005. Pre-eruptive
569 migration of earthquakes at the Piton de la Fournaise volcano (Réunion Island). Geophys.
570 J. Int., 161(2): 549-558.

571 Bean, C., Lokmer, I. and O'Brien, G., 2008. Influence of near-surface volcanic structure on long-
572 period seismic signals and on moment tensor inversions: Simulated examples from
573 Mount Etna. J. Geophys. Res., 113(B8): B08308.

574 Brenguier, F., Kowalski, P., Staudacher, T., Ferrazzini, V., Lauret, F., Boissier, P., Catherine, P.,
575 Lemarchand, A., Pequegnat, C., Meric, O., Pardo, C., Peltier, A., Tait, S., Shapiro, N.M.,
576 Campillo, M. and Di Muro, A., 2012. First Results from the UnderVolc High Resolution
577 Seismic and GPS Network Deployed on Piton de la Fournaise Volcano. Seismol. Res.
578 Lett., 83(1): 97-102.

579 Chouet, B., 1996. Long-period volcano seismicity: its source and use in eruption forecasting.
580 Nature, 380(6572): 309-316.

581 Chouet, B., 2003. Volcano Seismology. Pure Appl. Geophys., 160(3): 739-788.

582 Davi, R., O'Brien, G.S., De Barros, L., Lokmer, I., Bean, C.J., Lesage, P., Mora, M.M. and Soto,
583 G.J., 2012. Seismic source mechanisms of tremor recorded on Arenal volcano, Costa
584 Rica, retrieved by waveform inversion. J. Volcanol. Geoth. Res., 213–214(0): 1-13.

De Barros, L., Bean, C.J., Lokmer, I., Saccorotti, G., Zuccarello, L., O'Brien, G.S., Métaxian, J.-P. and Patanè, D., 2009. Source geometry from exceptionally high resolution long period event observations at Mt Etna during the 2008 eruption. Geophys. Res. Lett., 36(24): L24305.

De Barros, L., Lokmer, I., Bean, C.J., O'Brien, G.S., Saccorotti, G., Métaxian, J.P., Zuccarello, L. and Patanè, D., 2011. Source mechanism of long-period events recorded by a high-density seismic network during the 2008 eruption on Mount Etna. J. Geophys. Res., 116(B1): B01304.

Fischer, T. and Guest, A., 2011. Shear and tensile earthquakes caused by fluid injection. Geophys. Res. Lett., 38(5): L05307.

Got, J.L., Fréchet, J. and Klein, F.W., 1994. Deep fault plane geometry inferred from multiplet relative relocation beneath the south flank of Kilauea. J. Geophys. Res., 99(B8): 15375-15386.

Gouhier, M. and Coppola, D., 2011. Satellite-based evidence for a large hydrothermal system at Piton de la Fournaise volcano (Reunion Island). Geophysical Research Letters, 38(2): L02302.

Green, D.N. and Neuberg, J., 2006. Waveform classification of volcanic low-frequency earthquake swarms and its implication at Soufrière Hills Volcano, Montserrat. Journal of Volcanology and Geothermal Research, 153(1–2): 51-63.

Kumagai, H., Chouet, B.A. and Dawson, P.B., 2005. Source process of a long-period event at Kilauea volcano, Hawaii. Geophys. J. Int., 161(1): 243-254.

606 Kumagai, H., Chouet, B.A. and Nakano, M., 2002. Waveform inversion of oscillatory signatures
607 in long-period events beneath volcanoes. J. Geophys. Res., 107(B11): 2301.

608 Kumagai, H., Saito, T., O'Brien, G. and Yamashina, T., 2011. Characterization of scattered
609 seismic wavefields simulated in heterogeneous media with topography. J. Geophys. Res.,
610 116(B3): B03308.

611 Lénat, J.-F., Fitterman, D., Jackson, D.B. and Labazuy, P., 2000. Geoelectrical structure of the
612 central zone of Piton de la Fournaise volcano (Réunion). Bulletin of Volcanology, 62(2):
613 75-89.

614 Lokmer, I., Bean, C.J., Saccorotti, G. and Patanè, D., 2007. Moment-tensor inversion of LP
615 events recorded on Etna in 2004 using constraints obtained from wave simulation tests.
616 Geophys. Res. Lett., 34(22): L22316.

617 Massin, F., Ferrazzini, V., Bachèlery, P., Nercessian, A., Duputel, Z. and Staudacher, T., 2011.
618 Structures and evolution of the plumbing system of Piton de la Fournaise volcano
619 inferred from clustering of 2007 eruptive cycle seismicity. J. Volcanol. Geoth. Res.,
620 202(1-2): 96-106.

621 Matoza, R.S. and Chouet, B.A., 2010. Subevents of long-period seismicity: Implications for
622 hydrothermal dynamics during the 2004–2008 eruption of Mount St. Helens. Journal of
623 Geophysical Research: Solid Earth, 115(B12): B12206.

624 McNutt, S.R., 2000. Seismic Monitoring. In: H. Sigurdsson (Editor), Encyclopedia of Volcanoes.
625 Academic Press, San Diego, pp. 1095-1119.

McNutt, S.R., 2005. Volcanic Seismology. Annu. Rev. Earth Pl. Sc., 33(1): 461-491.

Michon, L., Staudacher, T., Ferrazzini, V., Bachèlery, P. and Marti, J., 2007. April 2007 collapse of Piton de la Fournaise: A new example of caldera formation. Geophys. Res. Lett., 34(21).

Nakano, M. and Kumagai, H., 2005. Waveform inversion of volcano-seismic signals assuming possible source geometries. Geophys. Res. Lett., 32(12): L12302.

Nercessian, A., Hirn, A., Lépine, J.-C. and Sapin, M., 1996. Internal structure of Piton de la Fournaise volcano from seismic wave propagation and earthquake distribution. J. Volcanol. Geoth. Res., 70(3–4): 123-143.

Neuberg, J.W., Tuffen, H., Collier, L., Green, D., Powell, T. and Dingwell, D., 2006. The trigger mechanism of low-frequency earthquakes on Montserrat. J. Volcanol. Geoth. Res., 153(1–2): 37-50.

O'Brien, G.S. and Bean, C.J., 2004. A 3D discrete numerical elastic lattice method for seismic wave propagation in heterogeneous media with topography. Geophys. Res. Lett., 31(14).

Ohminato, T., Chouet, B.A., Dawson, P. and Kedar, S., 1998. Waveform inversion of very long period impulsive signals associated with magmatic injection beneath Kilauea Volcano, Hawaii. J. Geophys. Res., 103(B10): 23839-23862.

OVPF report, 2010. Rapport d'activité 2010. Institut de Physique du Globe de Paris, Observatoire Volcanologique du Piton de la Fournaise, http://www.ipgp.fr/files_lib/930_RapportActivite2010-02-12.pdf.

Peltier, A., Bachèlery, P. and Staudacher, T., 2009. Magma transport and storage at Piton de La Fournaise (La Réunion) between 1972 and 2007: A review of geophysical and geochemical data. J. Volcanol. Geoth. Res., 184(1–2): 93-108.

Peltier, A., Ferrazzini, V., Staudacher, T. and Bachèlery, P., 2005. Imaging the dynamics of dyke propagation prior to the 2000-2003 flank eruptions at Piton de La Fournaise, Reunion Island. Geophys. Res. Lett., 32(22): L22302.

Peltier, A., Massin, F., Bachèlery, P. and Finizola, A., 2012. Internal structure and building of basaltic shield volcanoes: the example of the Piton de La Fournaise terminal cone (La Réunion). Bulletin of Volcanology, 74(8): 1881-1897.

Peltier, A., Staudacher, T. and Bachèlery, P., 2007. Constraints on magma transfers and structures involved in the 2003 activity at Piton de La Fournaise from displacement data. J. Geophys. Res., 112(B3).

Saccorotti, G., Chouet, B. and Dawson, P., 2001. Wavefield properties of a shallow long-period event and tremor at Kilauea Volcano, Hawaii. J. Volcanol. Geoth. Res., 109(1–3): 163-189.

Saccorotti, G., Chouet, B. and Dawson, P., 2003. Shallow-velocity models at the Kilauea Volcano, Hawaii, determined from array analyses of tremor wavefields. Geophys. J. Int., 152(3): 633-648.

Saccorotti, G., Lokmer, I., Bean, C.J., Di Grazia, G. and Patanè, D., 2007. Analysis of sustained long-period activity at Etna Volcano, Italy. J. Volcanol. Geoth. Res., 160(3-4): 340-354.

666 Saccorotti, G., Zuccarello, L., Del Pezzo, E., Ibanez, J. and Gresta, S., 2004. Quantitative
667 analysis of the tremor wavefield at Etna Volcano, Italy. J. Volcanol. Geoth. Res., 136(3–
668 4): 223-245.

669 Shearer, P.M., 1997. Improving local earthquake locations using the L1 norm and waveform
670 cross correlation: Application to the Whittier Narrows, California, aftershock sequence. J.
671 Geophys. Res., 102(B4): 8269-8283.

672 Staudacher, T., 2010. Field observations of the 2008 summit eruption at Piton de la Fournaise
673 (Ile de La Réunion) and implications for the 2007 Dolomieu collapse. J. Volcanol. Geoth.
674 Res., 191(1-2): 60-68.

675 Staudacher, T., Ferrazzini, V., Peltier, A., Kowalski, P., Boissier, P., Catherine, P., Lauret, F. and
676 Massin, F., 2009. The April 2007 eruption and the Dolomieu crater collapse, two major
677 events at Piton de la Fournaise (La Réunion Island, Indian Ocean). J. Volcanol. Geoth.
678 Res., 184(1–2): 126-137.

679 Taisne, B., Brenguier, F., Shapiro, N.M. and Ferrazzini, V., 2011. Imaging the dynamics of
680 magma propagation using radiated seismic intensity. Geophys. Res. Lett., 38(4): L04304.

681 Takei, Y. and Kumazawa, M., 1995. Phenomenological representation and kinematics of general
682 seismic sources including the seismic vector modes. Geophys. J. Int., 121(3): 641-662.

683 Vasco, D.W., 1989. Deriving source-time functions using principal component analysis. B.
684 Seismol. Soc. Am., 79(3): 711-730.

685 Vavrycuk, V., 2001. Inversion for parameters of tensile earthquakes. J. Geophys. Res., 106(B8):
686 16339-16355.

687 Venzke, E., Sennert, S., Wunderman, R. and Carter, C., 2010. Reports from the Smithsonian's
688 Global Volcanism Network, March 2010. B. Volcanol., 72(7): 889-891.

689 Waldhauser, F. and Ellsworth, W.L., 2000. A Double-Difference Earthquake Location
690 Algorithm: Method and Application to the Northern Hayward Fault, California. B.
691 Seismol. Soc. Am., 90(6): 1353-1368.

692

Figure Captions

Figure 1. *Inset:* Location of La Réunion Island. *Main:* Broadband seismic station locations on Piton de la Fournaise volcano, La Réunion Island.

Figure 2. Temporal Distribution of LP events between November 2009 and January 2011. Note that not all eruptions have LP events associated with them, and that in late September 2010 several LP events were recorded during a seismic crisis but no eruption took place; this period is known as an intrusive phase. LP events are numbered in chronological order. Amplitude is the maximum amplitude of the trace recorded on the vertical component of station U05, filtered between 0.5 and 4 Hz.

Figure 3. The 15 LP events that were recorded on Piton de la Fournaise volcano are normalized and shown in the left panel, with grey illustrating the unfiltered signal and red illustrating the filtered waveform, band-passed between 0.5 and 4 Hz. The spectral content of each of the unfiltered LP events is shown in the right panel; note that most of the energy is found between 2 and 4 Hz.

Figure 4. A family of three LP events (normalized and filtered between 0.5-4.0 Hz) with highly correlated waveforms, recorded on the vertical component of stations U05 and U11 during the September 2010 seismic crisis.

Figure 5. Locations of a family of LP events using picked (PK) first-arrival times (solid symbols) and adjusted first-arrival times from double-difference (DD) method (open symbols), for a homogeneous velocity model of 3500 ms^{-1}. Error bars illustrate the extent of locations that had a misfit value within 5% of the minimum misfit of the most probable location (solid lines for PK location errors and dashed lines for DD location error. Views are from above (top panel), South (bottom left panel) and West (bottom right panel).

Figure 6. Results of Moment tensor inversion including single forces. *(a)* Source-time functions for six moment-tensor components and single forces of LP5 filtered between 0.7 and 1.8 Hz. *(b)* LP5 waveform fits for the three components (*left-right:* East, North and Vertical) of all stations, filtered between 0.7 and 1.8 Hz. Real data is shown in light blue and the synthetic data is shown in red. Note that the waveforms take M_0 into account. *(c)* Eigenvector plot illustrating the orientation of the source mechanism for all LP events (*left-right:* LP4, LP5 and LP7).

Figure 7. Seismic crisis recorded on station U05 on Piton de la Fournaise volcano for a) an intrusive phase on 23rd September 2010 and b) a volcanic eruption on 14th October. Red arrows indicate the position of LP events. Notice how the LP events are recorded towards the end of the seismic crisis, after the seismicity rate has peaked. NB. In order to see details within the seismogram the y-scale of these images are clipped. The maximum recorded amplitudes of the VT events during these crises were $2.4x10^{-3}$ mms^{-1} and $5.7x10^{-3}$ mms^{-1} for September and October respectively.

Table Captions

Table 1. Results of Unconstrained and Crack-Constrained Moment Tensor Inversion for LP5[a], for Source Depths of 50 m and 200 m. The results corresponding to Figure 6 are shown in italics.

[a]Here θ and φ are the dip angle from upwards vertical and the azimuth angle anti-clockwise from east (x), respectively, of the principal axis of the source mechanism; MagX, MagY and MagZ are the magnitudes of the M_{xx}, M_{yy} and M_{zz} moment tensor components, respectively; ISO, CLVD and DC describe the percentage of the source mechanism that is isotropic, compensated linear vector dipoles or double-couple, respectively; Res is the residual misfit between observed waveforms and reconstructed waveforms. The entry at 200 m depth of inversion type Unconstrained$^{(1)}$ is for an unconstrained inversion with the three summit stations (U05, U11 and SNE) jackknifed from the inversion.

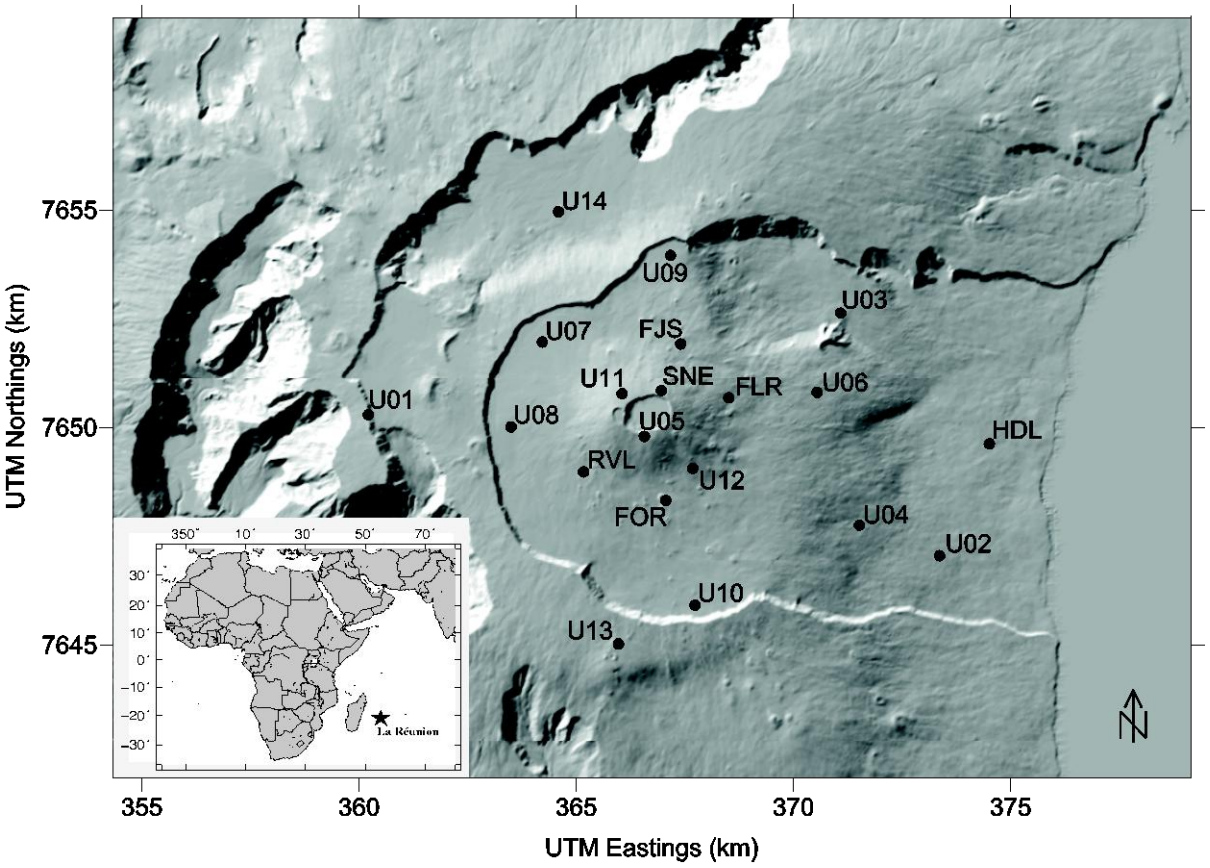
U14
U09
U03
U07
FJS
U11
SNE
FLR
U06
U01
U08
U05
HDL
RVL
U12
FOR
U04
U02
U10
U13
7655
7650
7645
355
360
365
370
375
UTM Northings (km)
UTM Eastings (km)
350°
10°
30°
50°
70°
30°
20°
10°
0°
-10°
-20°
-30°
La Réunion

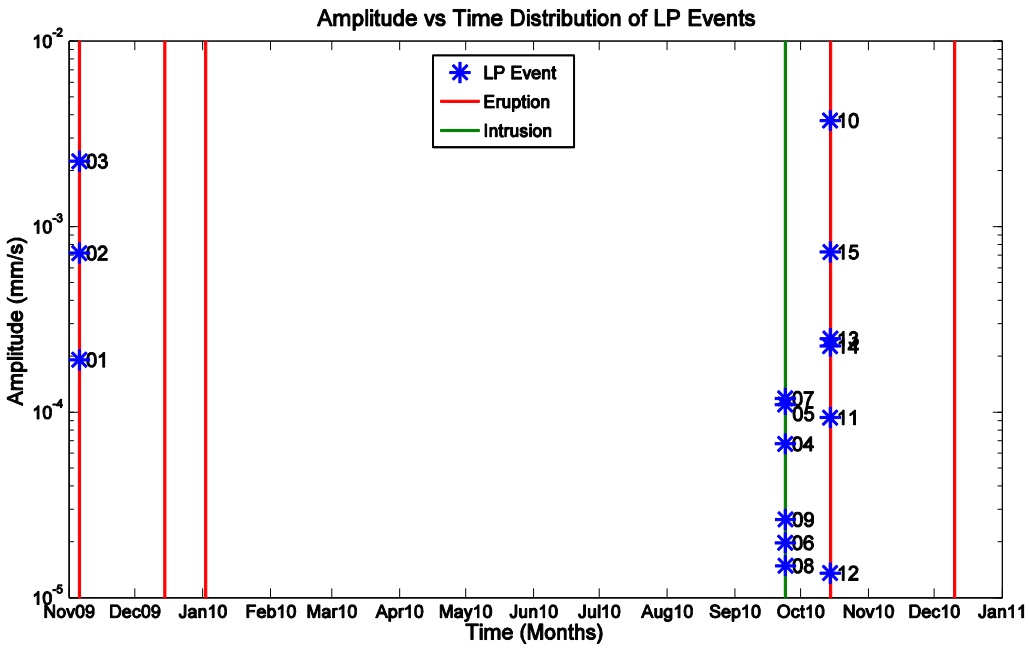
Amplitude vs Time Distribution of LP Events
LP Event
Eruption
Intrusion
Amplitude (mm/s)
Time (Months)
Nov09
Dec09
Jan10
Feb10
Mar10
Apr10
May10
Jun10
Jul10
Aug10
Sep10
Oct10
Nov10
Dec10
Jan11
01
02
03
04
05
06
07
08
09
10
11
12
13
14
15

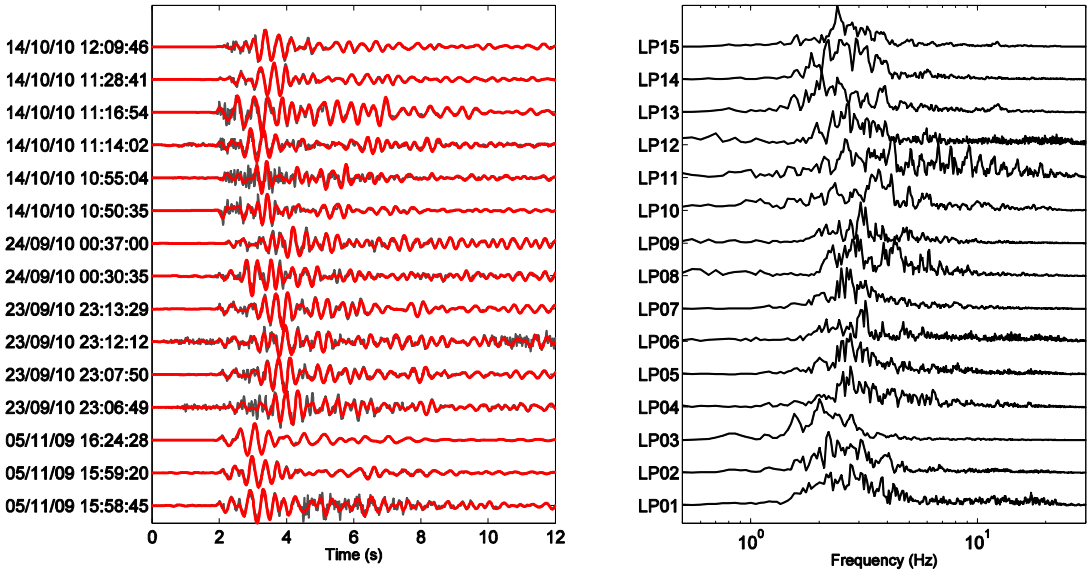
14/10/10 12:09:46
14/10/10 11:28:41
14/10/10 11:16:54
14/10/10 11:14:02
14/10/10 10:55:04
14/10/10 10:50:35
24/09/10 00:37:00
24/09/10 00:30:35
23/09/10 23:13:29
23/09/10 23:12:12
23/09/10 23:07:50
23/09/10 23:06:49
05/11/09 16:24:28
05/11/09 15:59:20
05/11/09 15:58:45
0
2
4
6
8
10
12
Time (s)
LP15
LP14
LP13
LP12
LP11
LP10
LP09
LP08
LP07
LP06
LP05
LP04
LP03
LP02
LP01
10^0
10^1
Frequency (Hz)

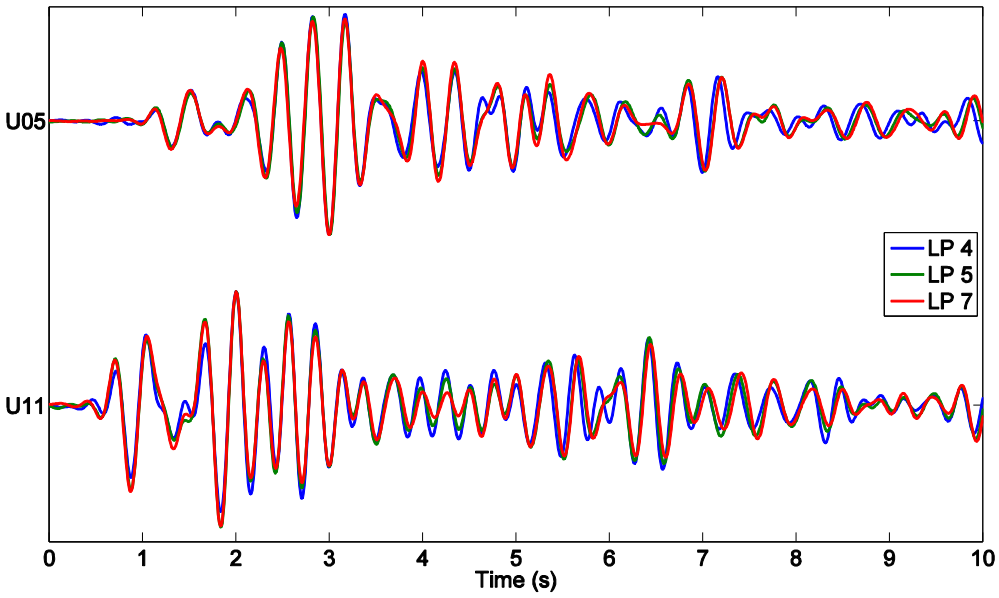
U05
U11
LP 4
LP 5
LP 7
0
1
2
3
4
5
6
7
8
9
10
Time (s)

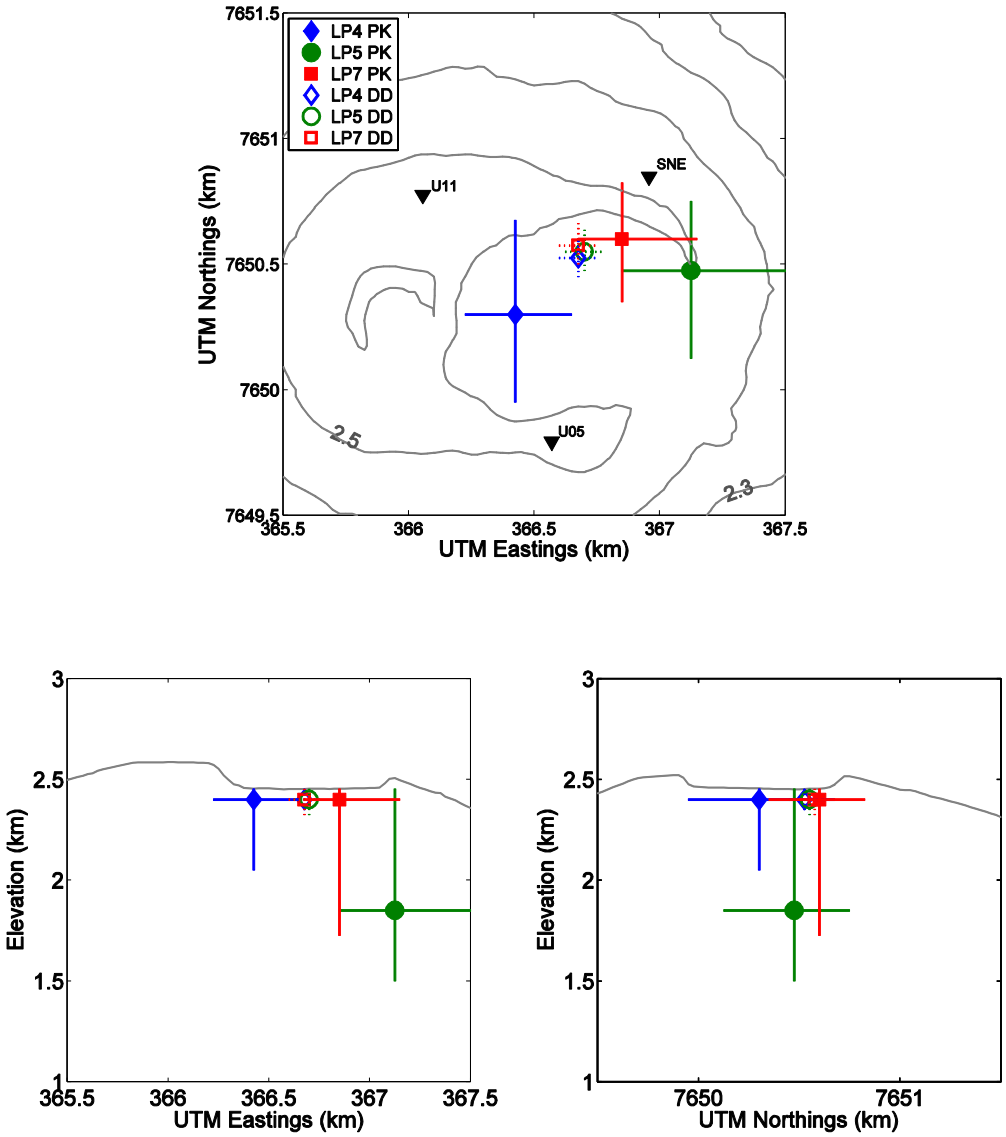
LP4 PK
LP5 PK
LP7 PK
LP4 DD
LP5 DD
LP7 DD
U11
SNE
U05
2.5
2.3
UTM Northings (km)
UTM Eastings (km)
Elevation (km)
UTM Eastings (km)
Elevation (km)
UTM Northings (km)

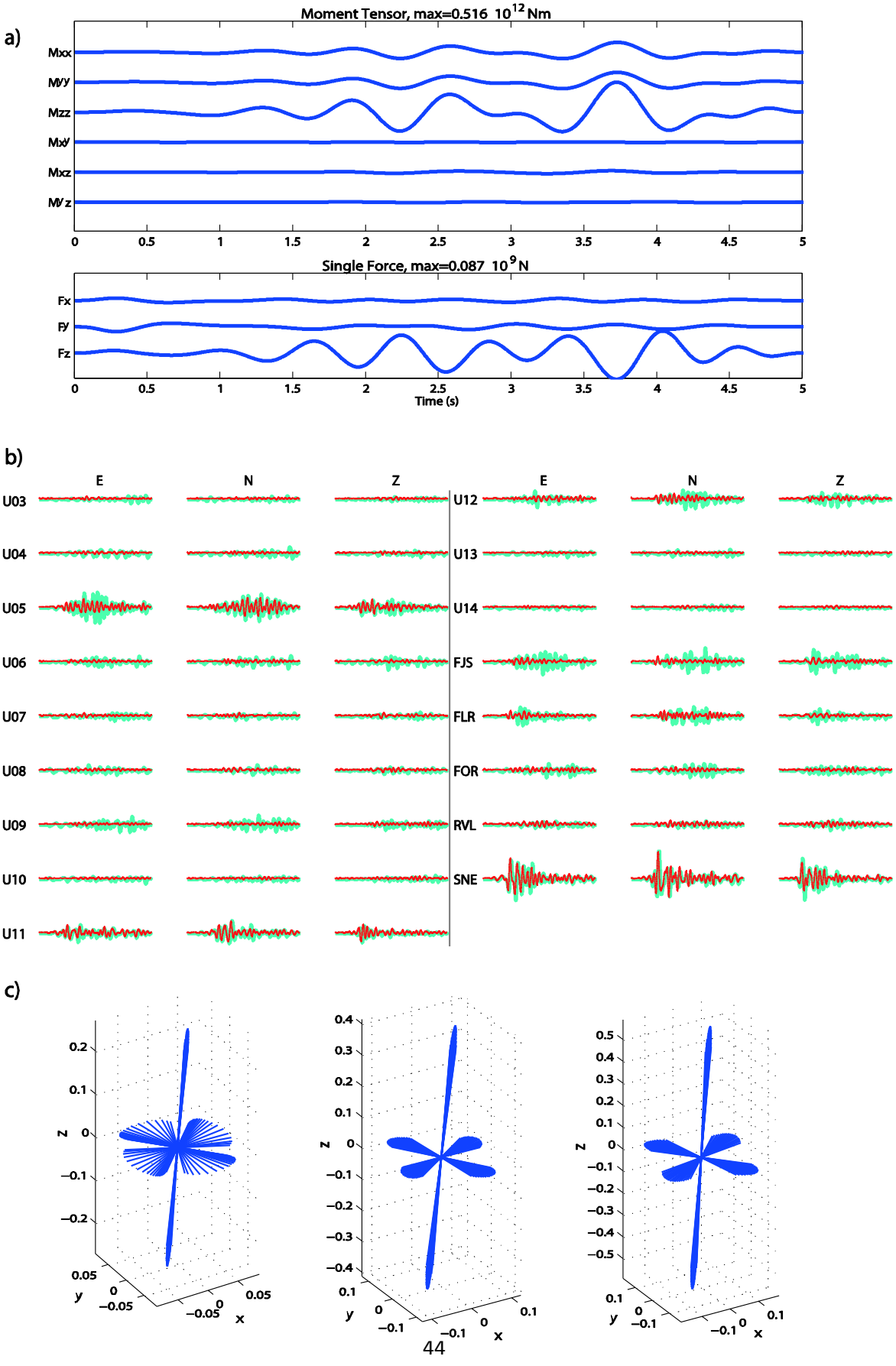
a)
Moment Tensor, max=0.516 10^12 Nm
Mxx
Myy
Mzz
Mxy
Mxz
Myz
Single Force, max=0.087 10^9 N
Fx
Fy
Fz
Time (s)
b)
E
N
Z
U03
U04
U05
U06
U07
U08
U09
U10
U11
U12
U13
U14
FJS
FLR
FOR
RVL
SNE
c)

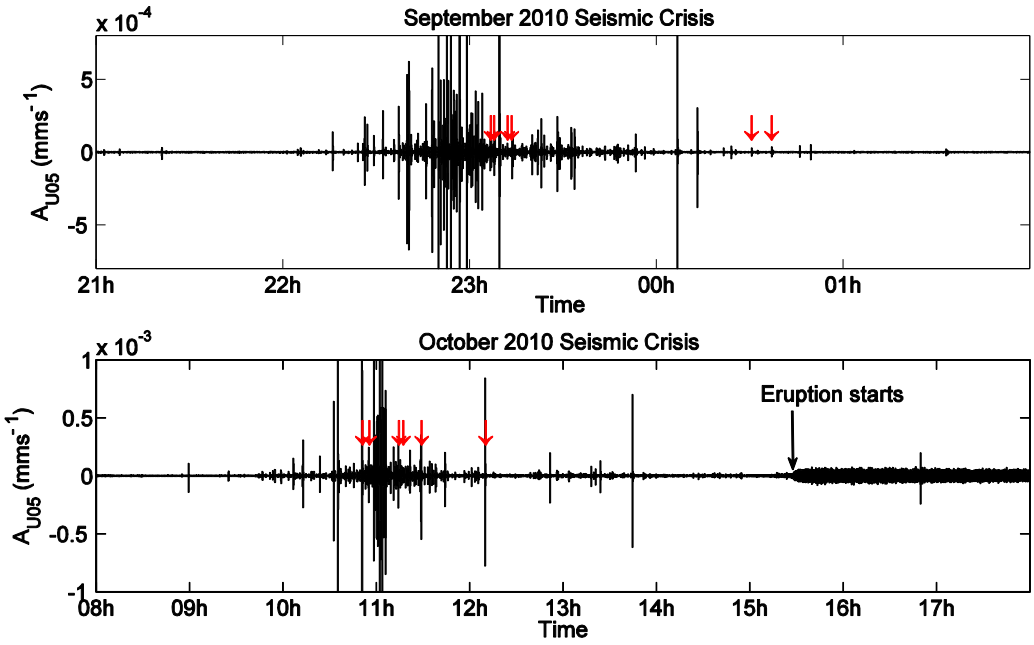
September 2010 Seismic Crisis
x 10^-4
A_U05 (mms^-1)
5
0
-5
21h
22h
23h
00h
01h
Time
October 2010 Seismic Crisis
x 10^-3
A_U05 (mms^-1)
1
0.5
0
-0.5
-1
Eruption starts
08h
09h
10h
11h
12h
13h
14h
15h
16h
17h
Time

MTI with single forces											
Type of Inversion	**Depth (m)**	**λ/μ**	**θ (°)**	**φ (°)**	**MagX**	**MagY**	**MagZ**	**ISO (%)**	**CLVD (%)**	**DC (%)**	**Res**
Unconstrained	50		5	8	1.0	1.01	3.09	55.0	44.6	0.4	0.63
Constrained Crack	50	1.0	10	20	1.0	1.0	3.0	55.6	44.4	0.0	0.77
Unconstrained	200		7	343	1.0	1.27	5.37	47.4	47.6	5.0	0.62
Unconstrained[(1)]	200		2	331	1.0	1.05	2.73	58.4	39.9	1.7	0.67
Constrained Crack	200	1.0	20	30	1.0	1.0	3.0	55.6	44.4	0.0	0.77
MTI without single forces											
Type of Inversion	**Depth (m)**	**λ/μ**	**θ (°)**	**φ (°)**	**MagX**	**MagY**	**MagZ**	**ISO (%)**	**CLVD (%)**	**DC (%)**	**Res**
Unconstrained	50		4	11	1.0	1.03	3.45	52.9	46.2	0.9	0.75